A. DI GERLANDO, R. PERINI, A. SILVESTRI, M. UBALDINI

DESIGN CRITERIA AND PERFORMANCE ANALYSIS OF PASSIVE PERMANENT MAGNET ELECTRO-INDUCTIVE DEVICES FOR SEISMIC VIBRATIONS DAMPING

Proceedings of the International Conference on
Electrical Machines
ICEM 2000

August 28-30, 2000
Espoo, Finland

INTERNATIONAL CONFERENCE ON ELECTRICAL MACHINES

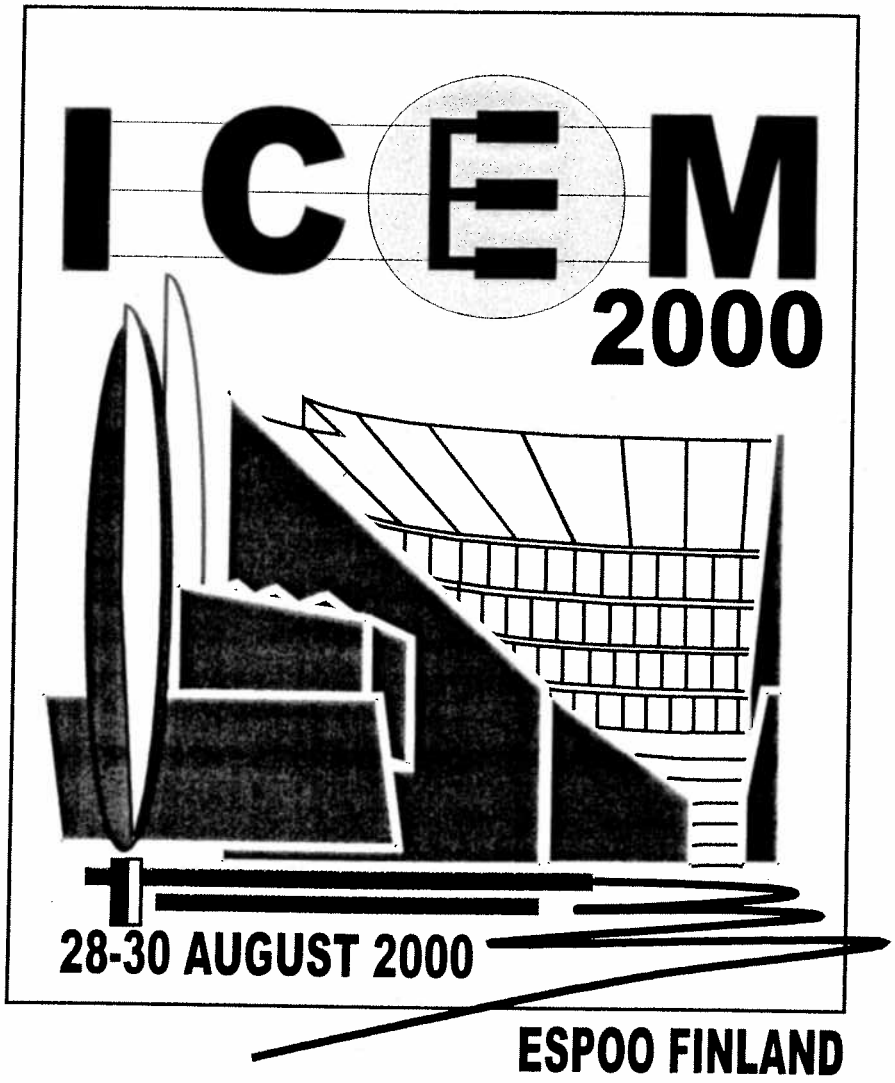

HELSINKI UNIVERSITY OF TECHNOLOGY

ESPOO FINLAND

Helsinki University of Technology
Espoo Finland

Design criteria and performance analysis of passive permanent magnet electro-inductive devices for seismic vibrations damping

A. Di Gerlando, R. Perini, A. Silvestri, M. Ubaldini

Dipartimento di Elettrotecnica - Politecnico di Milano
Piazza Leonardo da Vinci, 32 - 20133 Milano, Italy
Telephone: +39 02 23993722
Fax +39 02 23993703
E-mails: [diger, perini, silvestri, ubaldini]@bottani.etec.polimi.it

ABSTRACT

A special permanent magnet, passive device is described, to be employed for damping the vibrations of civil and industrial structures caused by earthquakes. The integrated electromagnetic-thermal model of this damper is developed, for design purposes and performance analysis.

Keywords: PM dampers, modelling, electromagnetic design.

1 INTRODUCTION

Many systems require the use of devices suited to damp vibrations, whose intensity and persistence could cause structural damages or trouble to people: a significant, even if not exclusive, sector is that of the civil and industrial structures protection from the earthquake effects. For this application, mechanical devices are currently in use (elasto-plastic dissipators, rubber insulators), but they show some disadvantages, among which fatigue and ageing phenomena, non-linearities and need of substitution after each important seismic event.

Thus, a research for the development of electromagnetic damping devices has been started, equipped with permanent magnet (PM) inductors (in the following each device will be called DECS = Device of Electro-inductive type for the Control of Structures). The research presents several interdisciplinary elements (sizing and electromechanical optimisation aspects, structural dynamics problems, economical aspects, tests): the activity, supported by the Italian Ministry of University & Research in Science and Technology (MURST), is in progress [1] and it involves some academic and research organisations and one firm (ALGA S.p.A., Milano, Italy).

While a DECS may have different configurations (linear or rotating, with flat or cylindrical air-gap, single or double sided,...) and operating principles (passive, semi-active, active kinds), this paper concerns the electromagnetic and thermal modelling aspects for the design of a passive DECS, equipped with a rotating, disk shaped, solid secondary.
A passive DECS is a damping device to be inserted among two parts of the structure to be protected, that are in relative linear alternative motion because of the seismic vibrations: during this motion the magnetic field produced by the PMs crosses a conductive, non-magnetic secondary, with development of eddy currents, thanks to the Faraday's law. Even if the operating principle is well known (all the eddy current braking devices are based on it), several structural and performance requirements make their design quite special: simplicity and robustness, independence from energy external sources and, above all, suitability to damp vibrations during phenomena characterised by short duration but high power intensity.

2 STRUCTURE OF THE PM PASSIVE DECS

The natural linear speed v_s of the seismic event is too low to give a sufficient damping effect: thus, the DECS requires a suited cinematic coupling (endless screw), for the linear-to-rotational motion transformation, with a speed multiplication.
The electromagnetic part of the DECS has a sandwich structure (fig.1): the stator, containing the solid secondary disk, is equipped with a double sided inductor (with axially aligned Neodymium Iron Boron PMs, alternatively magnetized along the periphery and disposed on ferromagnetic plates as circular belts centered around the rotation axis); the disk, driven by the endless screw, is crossed by the PMs field, and represents the induced circuit, in which all the power loss is developed.

The last aspect, in particular, represents an important constraint for the DECS sizing: the short duration of the phenomenon (a few ten seconds) implies a quick rise of the disk temperature, practically in an adiabatic mode: this fact involves relevant problems about operation and integrity of various parts of the device (disk metal, PMs, endless screw parts).

The design parameters are a lot: PM sizes and number (linked to the e.m.f.s frequency, once defined the speed); disk width, external and internal diameters in active belt; disk material (conductive, but not ferromagnetic, in order to avoid any attractive force, that could damage the support systems).
The definition of these parameters in such a way to obtain the desired performances limiting the DECS mass, sizes and cost, requires to develop a suited model of this device. The remarkable non-uniformity of the magnetic field crossing the thick disk, together with the relevant eddy currents reaction effects, make difficult a purely analytical approach to an accurate electromagnetic model (also considering the inherently 3D structure); on the other hand, a merely numerical analysis, based on Finite Element Method (FEM) simulations, appears

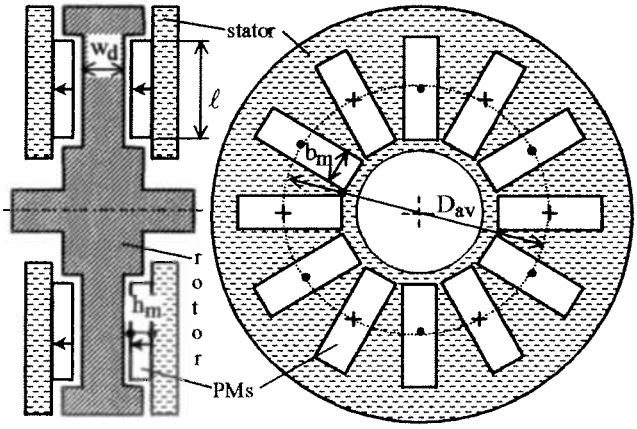

Fig. 1. Structure of a rotating, PM passive DECS.

both of limited cognitive value and difficult to be performed, not only for the numerous parameters, but also for the strict coupling with the thermal aspects. For these reasons, at first a simplified approach has been adopted, in which a basic analytical model is developed, whose inaccuracies are subsequently mitigated by employing corrective functions, validated by selected FEM simulations.

3 PM PASSIVE DECS ELECTROMAGNETIC MODEL

3.1 The basic, one-dimensional analytical model

By observing the DECS from an external radial direction, the scheme of fig.2 can be traced, where the shown peripheral sizes are measured along the average diameter D_{av}; the radial extension ℓ of the PMs is assumed equal to the radial extension of the induced portion of the disk (the active belt).
The hypotheses adopted for the model development are:
- field symmetry referred to the disk half width $d = w_d/2$;
- due to the PMs divergence, the field changes in radial direction: the model refers to the active belt average diameter;
- the section of the eddy current closing paths outside the active belt allows to neglect the corresponding voltage drop;
- even if the flux density inside the active belt has axial B_y and peripheral B_x components, just B_y is considered.

The last hypothesis, typically adopted in all the analytical models of electromagnetic devices, could appear too rough in this context, but it is correct. In fact, consider the disk in motion, with an average peripheral speed v (measured at D_{av}); called Ω [rad/s] the instantaneous rotational speed, we have:

$$v = \Omega \cdot D_{av}/2 = \Omega \cdot p \cdot \tau/(2 \cdot \pi) \quad , \qquad (1)$$

with p = number of PMs per side, τ = pole pitch (at D_{av}).
Indicated with ρ the disk resistivity, the specific power p developed in a point Q of the active belt is linked to speed, flux density and induced current density vectors as follows:

$$p = \rho \cdot \vec{J}_Q \bullet \vec{J}_Q = \left(\vec{v}_Q \times \vec{B}_Q\right) \bullet \left(\vec{v}_Q \times \vec{B}_Q\right)/\rho = B_{Qy}^2 \cdot v_Q^2/\rho \qquad (2)$$

Integrating eq. (2) within the disk active belt volume V_b gives the total power loss in the disk (writing B_y instead of B_{Qy}):

$$P = \int_{V_b} p \cdot dV_b \approx \ell \cdot p \cdot \left(v^2/\rho\right) \cdot \int_{A_{b\tau}} B_y^2 \cdot dA_{b\tau} \qquad (3)$$

with $A_{b\tau} = w_d \cdot \tau$ average cross section of one pole.
Eq.s (2) and (3) confirm that just B_y is effective.

FEM analyses showed that B_y depends on x and y: the x-dependence is alternated, with a trapezoidal shape; the y-dependence is the more important the greater the disk width w_d is. In the basic model, the axial variation of B_y is neglected, and the B_y peripheral distribution is assumed sinusoidal, as like as all the other spatial quantities concerning the active belt (m.m.f.s, current density distribution, ...).
Thus, indicate with $B_\delta(\theta)$ the axial flux density distribution B_y in the air-gap and in the disk, resultant of the effects of the PMs and of the eddy currents; B_δ is assumed independent on y in the disk width. The angular variable θ (in electrical radians) is measured in a rotating frame, synchronous with the disk,

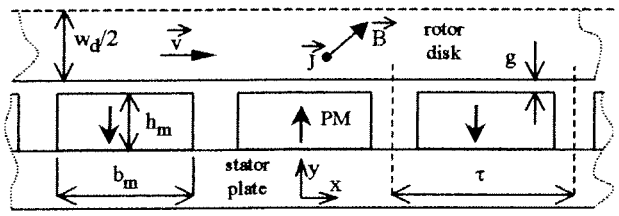

Fig. 2. Main sizes of the PM passive DECS, along the diameter D_{av}.

whose origin is chosen in the peripheral position where B_δ is zero with positive slope; called ξ the linear peripheral variable corresponding to x in the rotating frame, we have:

$$B_\delta(\theta) = B_{\delta_M} \cdot \sin(\theta) = B_{\delta_M} \cdot \sin(\pi \cdot \xi/\tau) \quad , \qquad (4)$$

where B_{δ_M} is the peak air-gap flux density.
The superficial current density induced in the disk is given by:

$$J(\theta) = B_\delta(\theta) \cdot v/\rho = B_{\delta_M} \cdot (v/\rho) \cdot \sin(\theta) \quad , \qquad (5)$$

and the corresponding linear current density distribution (referred to $d = w_d/2$, considering one air-gap crossing) equals:

$$\Delta(\theta) = d \cdot J(\theta) = d \cdot B_{\delta_M} \cdot (v/\rho) \cdot \sin(\theta) \quad . \qquad (6)$$

The m.m.f. $M_e(\theta)$ due to the eddy currents in the disk is the peripheral integral of $\Delta(\theta)$:

$$M_e(\xi) = \int \Delta(\xi) \cdot d\xi = \frac{\tau}{\pi} \cdot \int \Delta(\theta) \cdot d\theta = -M_{e_M} \cdot \cos(\theta) \, , \qquad (7)$$

with $$M_{e_M} = v \cdot B_{\delta_M} \cdot d \cdot \tau/(\pi \cdot \rho) \quad . \qquad (8)$$

As regards the PM equivalent m.m.f. $M_m(\theta)$, considering that the corresponding flux density distribution is assumed sinusoidal, we can write:

$$M_m(\theta) = M_{m_M} \cdot \sin(\theta + \vartheta_m) \quad ; \qquad (9)$$

in eq. (9) ϑ_m is a spatial angular phase (whose value depends on the composition of the space phasors acting in each air-gap); the PM peak m.m.f. can be expressed as follows:

$$M_{m_M} = \gamma_m \cdot M_{mo} = \gamma_m \cdot H_o \cdot h_m \quad , \qquad (10)$$

where h_m is the axial PM height, H_o the coercitive force (by linear extrapolation of the PM B(H) curve), and γ_m is a suited corrective factor, to be determined subsequently, taking into account the non-sinusoidal field distribution within the disk.
Moreover, the air-gap peak flux density of eq. (4) can be expressed as a function of the peak resultant m.m.f. M_{δ_M}:

$$B_{\delta_M} = \mu_o \cdot M_{\delta_M}/\delta \quad , \qquad (11)$$

with δ equivalent magnetic air-gap, linked to the mechanical air-gap g by the following expression.

$$\delta = d + g + h_m/\mu_{mr} \quad ; \qquad (12)$$

where μ_{mr} is the PM p.u. reversible permeability ($\mu_{mr} \approx 1.06$).
When the disk speed is zero (no eddy currents), the flux density in the disk, due to the PM only, equals:

$$B_m(\theta) = B_{m_M} \cdot \sin(\theta + \vartheta_m) \qquad (13)$$

where: $$B_{m_M} = \mu_o \cdot M_{m_M}/\delta \, . \qquad (14)$$

The three sinusoidal m.m.f.s $M_m(\theta)$, $M_e(\theta)$ and $M_\delta(\theta)$ can be associated to corresponding space phasors, whose link is:

$$\overline{M}_{\delta_M} = \overline{M}_{m_M} + \overline{M}_{e_M} \, . \qquad (15)$$

From eq. (15), considering eq.s (4), (7), (11) and (14), the following fundamental ratio $b_\delta = B_{\delta_M}/B_{m_M}$ can be obtained:

$$b_\delta = \frac{B_{\delta_M}}{B_{m_M}} = \frac{M_{\delta_M}}{M_{m_M}} = \sqrt{1 - M_{e_M}^2/M_{m_M}^2} \quad . \qquad (16)$$

b_δ represents the p.u. peak operating air-gap flux density, referred to the zero speed value B_{m_M}.
By means of eq.s (8) and (14), the ratio M_{e_M}/M_{m_M} becomes:

$$M_{e_M}/M_{m_M} = \left(B_{\delta_M}/B_{m_M}\right) \cdot (v/V_c) \, , \qquad (17)$$

where $$V_c = \frac{2 \cdot \pi \cdot \delta}{\mu_o \cdot w_d \cdot \tau} \cdot \rho = \alpha_c \cdot \rho \quad , \qquad (18)$$

having the dimension of a speed, can be called characteristic speed of the DECS. The combination of (16) and (17) allows to obtain the p.u. operating peak flux density b_δ:

$$b_\delta = B_{\delta_M}/B_{m_M} = 1/\sqrt{1 + (v/V_c)^2} \quad . \qquad (19)$$

By inserting eq.s (4) and (19) into eq. (3) and observing that $dA_{b\tau} = w_d \cdot d\xi$ and that $p \cdot \tau = \pi \cdot D_{av}$, one obtains:

$$P = \frac{1}{2} \cdot \frac{\pi}{\rho} \cdot D_{av} \cdot w_d \cdot \ell \cdot \frac{B_{m_M}^2 \cdot v^2}{1+(v/V_c)^2} = \frac{K_m}{\rho} \cdot \frac{v^2}{1+(v/V_c)^2} \quad . \quad (20)$$

Eq. (20) shows that P does not depend on the number of poles, but only on the active belt volume ($V_b = \pi \cdot D_{av} \cdot \ell \cdot w_d$), on the peak value of the equivalent sinusoidal PM flux density (see eq. (14)) and on the peripheral speed v at D_{av}.

The seismic motion to be damped can be assumed as sinusoidal, with a mechanical period $T_s \approx 2$ s: thus, during each oscillation, the speed v is time dependent, according to the law:

$$v(t) = V_M \cdot \sin(2 \cdot \pi \cdot t/T_s) \quad ; \quad (21)$$

the speed is maximum in the central position of the rotation excursion, while it equals zero at the extreme positions, at the motion inversion points. Thus also the power P varies and, defined the speed ratio k_v as:

$$k_v = V_M / V_c \quad , \quad (22)$$

the average power within one seismic period T_s equals:

$$P_{av.s} = \frac{1}{T_s} \cdot \int_0^{T_s} P(v(t)) \cdot dt = \frac{K_m}{\rho} \cdot V_c^2 \cdot \left(1 - 1/\sqrt{1+k_v^2}\right) . \quad (23)$$

It is useful to evaluate the rms speed V_{rms}, i.e. that constant speed that, inserted in eq. (20), gives the average power expressed by eq. (23); from calculations, one obtains:

$$V_{rms} = V_M \cdot \sqrt{\sqrt{1+k_v^2} - 1} \Big/ k_v \quad ; \quad (24)$$

thus, the rms speed depends not only on the intrinsic features of the DECS, but also on the peak speed; the limit value of V_{rms} for very slow movements ($V_M << V_c \Rightarrow k_v \to 0$) equals $1/\sqrt{2}$, as can be realised by observing that the eddy current reaction disappears (see eq. (17)) and that the speed dependent term of eq. (20) becomes a squared sinusoidal function.

3.2 The corrective functions of the basic model

Eq.s (20) and (23) give the instantaneous and average DECS power, including the eddy current reaction effect, but they are an ideal model, because they do not consider that:

- the PM spatial field distribution is not sinusoidal;
- the field changes along the axial width w_d of the disk active belt;
- the eddy currents are not uniformly distributed (skin effect).

The first two inaccuracy causes can be partially mitigated by transforming eq. (3) as follows:

$$P = \ell \cdot p \cdot \frac{v^2}{\rho} \cdot \int_{A_{b\tau}} B_\delta^2 \cdot dA_{b\tau} \approx \frac{\ell \cdot p \cdot v^2/\rho}{1+(v/V_c)^2} \cdot \int_{A_{b\tau}} B_m^2 \cdot dA_{b\tau} \quad . \quad (25)$$

Eq. (25) assumes that the reaction effect deduced with a sinusoidal field distribution (eq. (19)) remains valid also for a non-sinusoidal, non-axially uniform field: this assumption is correct if the reaction effect is not strong (in fact, if $V_M << V_c$, then the second integral of eq. (25) tends to the first one).

By equating the second integral of eq. (25) to that of a sinusoidal distribution giving the same integral value, the equivalent peak PM sinusoidal flux density $B_{m_{Meq}}$ follows:

$$B_{m_{Meq}} = \sqrt{2} \cdot \sqrt{\frac{1}{A_{b\tau}} \cdot \int_{A_{b\tau}} B_m^2 \cdot dA_{b\tau}} = \sqrt{2} \cdot B_{m.rms} \quad (26)$$

where $B_{m.rms}$ is the space rms value flux density, produced within the disk width by the steady state PM magnetisation.

The knowledge of $B_{m_{Meq}}$ allows to calculate the corrective factor γ_m of eq. (10); in fact, if we define an ideal PM peak sinusoidal flux density $B_{m_{Mi}}$ as:

$$B_{m_{Mi}} = \mu_o \cdot M_{mo} / \delta \quad , \quad (27)$$

considering eq. (14) we can write:

$$\gamma_m = M_{m_M} / M_{mo} = B_{m_{Meq}} / B_{m_{Mi}} \quad . \quad (28)$$

$B_{m_{Meq}}$ has been calculated by means of FEM simulations and, by eq. (28), a dimensionless function has been deduced: considering that the design parameters are numerous, the parameter ratios considered were δ/τ and b_m/τ, while the mechanical gap and the PM height have been fixed (g = 1 mm and h_m = 10 mm, with τ = 40 mm; the variation range of b_m was 24÷38 mm and that of w_d was 2÷30 mm). The results of these calculations have been expressed in a numerical form, by defining suited cubic spline interpolating curves (fig. 3).

As regards the skin effect, a classical theory has been adopted [2]: it takes into account the penetration depth into the disk width, multiplying the material resistivity ρ by a corrective skin factor K_s, in such a way to correct the power:

$$K_s = \frac{w_d/2}{d_p} \cdot \frac{\sinh(w_d/d_p) + \sin(w_d/d_p)}{\cosh(w_d/d_p) - \cos(w_d/d_p)} \quad , \quad (29)$$

where d_p is the penetration depth:

$$d_p = \sqrt{\rho/(\pi \cdot \mu_o \cdot f)} \quad , \quad (30)$$

and $f = p \cdot \Omega/(4 \cdot \pi)$ is the internal frequency, time varying as the speed v (see eq. (21)); it is worth remarking that K_s is non linearly dependent on the material resistivity, i.e. $K_s = K_s(\rho)$.

4 PM PASSIVE DECS THERMAL MODEL

Taking into account eq.s (18), (20) and (29), the power equals:

$$P = \frac{K_m}{K_s(\rho) \cdot \rho} \cdot v^2 \Big/ \left[1 + \left(\frac{v}{\alpha_c \cdot \rho}\right)^2\right] \quad ; \quad (31)$$

the reason to show ρ explicitly in eq. (31) is that (proportionally to the temperature resistivity coefficient of the disk material) ρ changes with the instantaneous temperature, which increases quickly and significantly during the seismic event. In fact, it is important to consider the corresponding time power variation during the thermal transient, both for a correct damping evaluation and for a reliable thermal check.

Considering eq. (31), verified also by using magneto-static and eddy current Finite Element Analysis simulations, we have developed the DECS design and theoretically verified its thermal behavior during and after the seismic event: to this aim, an equivalent dynamical thermal network of the DECS has been studied, shown in fig.4.

This thermal model has been obtained by concentrating the continuous temperature distribution in suited thermal nodes: **a** is the room temperature node (40°C); **1**, **6**, **7** are disk nodes in the active belt, while **2** is a disk node within the base cylinder;

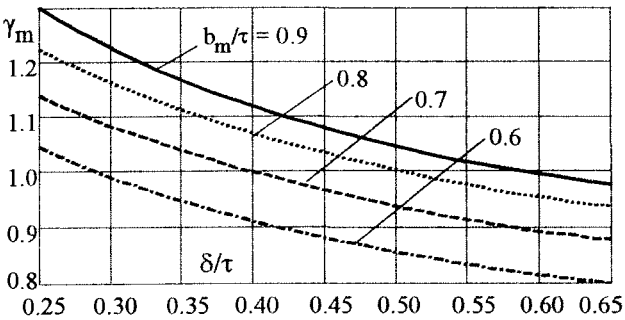

Fig. 3. Corrective function γ_m to be used in eq. (10).

3 is the thermal node representing the screw material; 4 is the surface magnet node towards the air gap, while **0** is the node at the contact between magnets and stator plates; the stator temperature towards the ambient is given by the node 5.
The network includes thermal conductances (modelling conductive, convective and radiation phenomena, at different speeds and thermal conditions), thermal capacitances (masses x specific heat parameters), and assumes the disk losses P concentrated in the average circumference of the active belt.

5 PM PASSIVE DECS SIMULATION EXAMPLES

By means of the described thermal network, a few simulations have been performed, in order to examine different design opportunities, such as sizes, materials, operating conditions.
Among several simulations, some results about two different disk designs will be discussed: aluminum disk and copper alloy disk with a nickel percentage equal to 11% (see Table I).

Table 1. Data of the passive PM DECS considered for the simulations

Rotating, passive PM DECS parameters [units]	Aluminum disk	Cu-Ni 11% disk
disk belt average diam. D_{av}; width w_d [mm]	420 ; 17	420 ; 10
disk fusion temp. T_f [°C]; $\rho_{20°C}$ [nΩm]	660; 26.6	1100; 150
resistivity temperature coefficient K_ρ [$°C^{-1}$]	0.0039	0.00049
endless screw speed multipl. factor (v / v_s)	13.2	13.2
mechanical air-gap g (per side) [mm]	1	1
PM N° (per side); peripheral size b_m [mm]	32; 30	32 ; 30
PM axial height h_m; radial length ℓ [mm]	10 ; 80	10; 80
PM material: Nd Fe B ; B_r [T] ; H_c [kA/m]	1.2 ; 900	1.2 ; 900
seismic quantities: V_M [m/s]; T_s [s]; Δt_s [s]	0.7; 2; 20	0.7; 2; 20

The main curves are shown in fig.5 (for aluminum disk DECS) and in fig.6 (for Cu-Ni alloy disk DECS), where the reference power P_r equals 125 kW. The following remarks can be made:
- figures 5a, 6a show the p.u. power loss P, estimated by (31), as a function of the seismic speed v_s, for three different disk temperatures T_d: it can be observed that in the conditions T_d = 115°C, v_s = 0.5 m/s, the aluminum disk DECS is capable to develop the reference power loss, while in the same conditions the Cu-Ni alloy disk DECS develops only 65 % of this loss; conversely, the alloy disk DECS is less sensitive to the disk temperature and it is less subjected to the demagnetizing effect of the induced currents: thus, it maintains a parabolic $P(v_s)$ behavior even at high speed values;

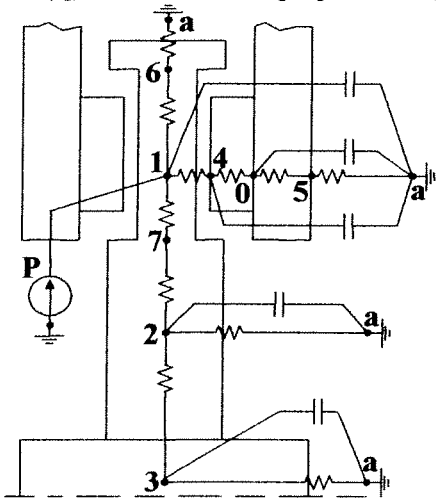

Fig.4. Schematic of the equivalent thermal network of the passive DECS shown in fig.1, with the node denominations.

- figures 5b, 6b show the p.u. instantaneous power loss and the highest disk temperature (in the belt center - node 1 -, referred to the material fusion temperatures), for a seismic event with the parameters of Table 1: the transients confirm the weaker temperature sensitivity of the alloy disk DECS, anyway capable to develop satisfying loss peak values; moreover, starting from $T_{ambient}$ = 40°C, disk temperatures

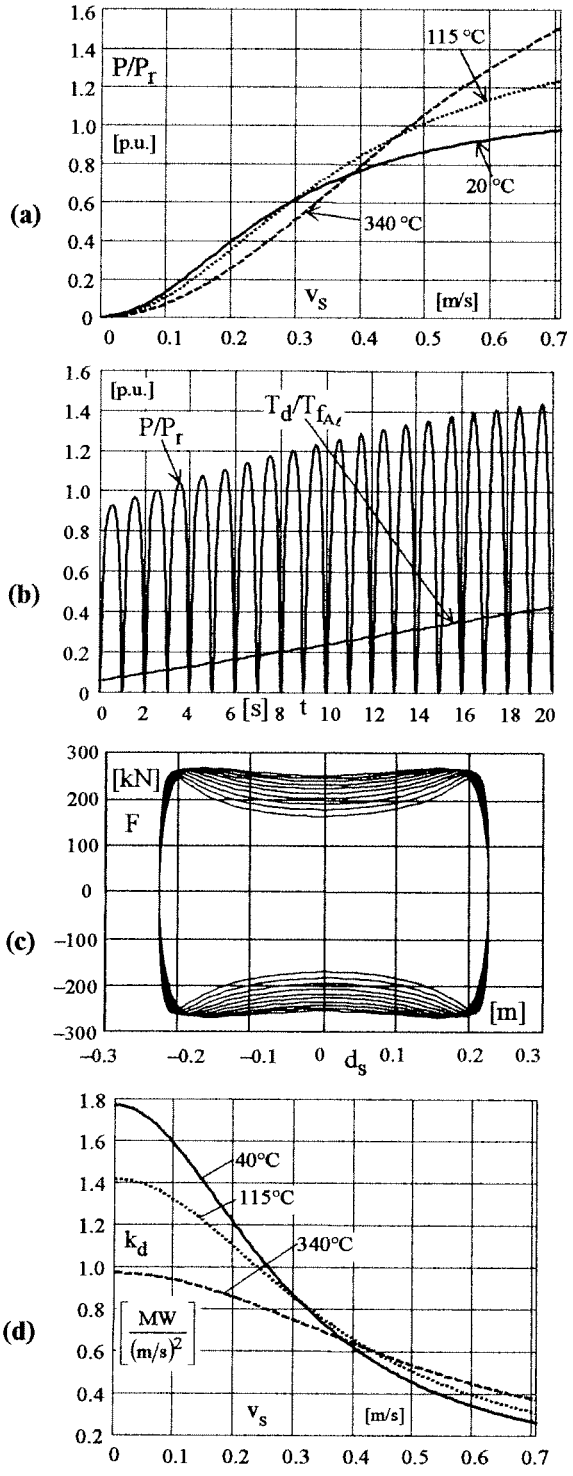

Fig. 5. Aluminum disk DECS simulated operating characteristics:
a: p.u. power loss P, as a function of the seismic speed v_s
b: instantaneous p.u. P and disk temperature (referred to the Al fusion temperature), for the seismic event of Table 1
c: force F – seismic displacement d_s cycles at the DECS hinges, during the simulated earthquake
d: damping parameter $k_d = P/v_s^2$, as a function of v_s.

rise quickly (reaching T_{dAlfin} = 340°C and T_{dCNfin} = 290°C for aluminum and alloy disks respectively), but they remain far from dangerous values, both during and after the seismic event; the same has been verified also for the magnets;

- curves 5c, 6c show the force F – seismic displacement d_s diagrams at the DECS hinges, during the simulated earthquake; the cited parabolic behavior of the alloy disk DECS (curves 6a) is confirmed by the quasi – elliptic shape of the corresponding force – displacement cyclic diagram;
- curves 5d, 6d show the damping parameter $k_d = P/v_s^2$, as a function of the speed v_s, with the disk temperature as a parameter: it is clear that the alloy DECS damping parameter is not far from a constant, while the aluminum disc DECS confirms a greater speed and temperature dependence.

Fig.s 5b and 6b show the great fluctuation of the instantaneous developed power P (that becomes zero at each motion inversion, every $T_s/2$ = 1 s, because of the seismic oscillation): this power variation does not produce appreciable ripple in the disk temperature rising waveform, thanks to the filtering effect of the disk thermal capacitance.

This remark allows to perform a very quick approximated evaluation of the disk temperature rise during the seismic event: in fact, if the average developed power $P_{av.s}$ of eq. (23) is considered, the final disk temperature T_{df} can be estimated as follows:

$$T_{df} \approx T_{di} + (1/C_{bd}) \cdot P_{av.s} \cdot \Delta t_s \quad , \qquad (32)$$

where T_{di} is the disk initial temperature, C_{bd} is the thermal capacitance of the disk active belt and $P_{av.s}$ can be evaluated at the average belt temperature T_{dav}:

$$T_{dav} \approx (T_{di} + T'_{df})/2 \quad ; \qquad (33)$$

in eq. (32), a first estimation T'_{df} of T_{df} is required, that can be obtained by inserting $P_{av.s}(T_{di})$ in eq. (32).

Calculations of T_{df} by eq. (32) for the two previous cases have shown differences of the order of few percent, compared with the calculations performed by the thermal transients.

6 CONCLUSIONS

A permanent magnet, passive, rotating damper for the control and protection of structures by the effects of seismic vibrations has been presented (DECS), equipped with devices for linear-to-rotational motion transformation.

An electromagnetic-thermal coupled model of this damper has been developed, useful for design calculations, parameter sensitivity analysis and estimation of operating performances.

The non sinusoidal, non uniform PM field distribution has been considered, together the skin effect and the thermal variation of the disk resistivity.

Characteristics evaluations and transient simulations have shown the suitability of these device to operate an effective damping action.

The research is in progress, for the design of other devices, the construction of prototypes and the experimental verification of their performances.

REFERENCES

[1] A. MARIONI, M. BATTAINI, G. DEL CARLO, F. CASCIATI, A. DI GERLANDO, R. PERINI, A. SILVESTRI, M. UBALDINI, "Development and Application of Electro-Inductive Dissipators". Proceedings of the International Post-SmirRT Conference Seminar on Seismic Isolation, Passive Energy Dissipation and Active Control of Vibrations of Structures, Cheju, Korea, 23-25 August 1999.

[2] S. A. NASAR, I. BOLDEA, "Linear Motion Electric Machines". John Wiley & Sons, New York, 1976, p.63.

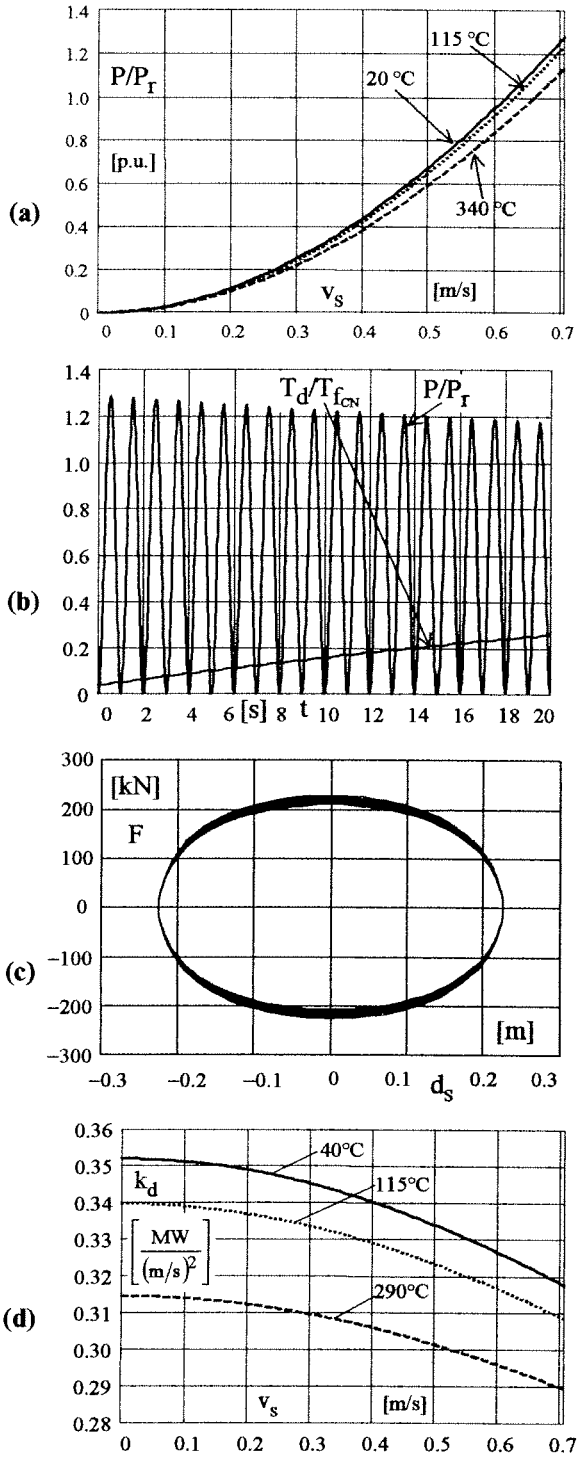

Fig. 6. Cu-Ni11% alloy disk DECS simulated operating characteristics:
a: p.u. power loss P, as a function of the seismic speed v_s
b: instantaneous p.u. P and disk temperature (referred to the alloy fusion temperature), for the seismic event of Table 1
c: force F – seismic displacement d_s cycles at the DECS hinges, during the simulated earthquake
d: damping parameter $k_d = P/v_s^2$, as a function of v_s.